

ФИЗИКА ПЛАЗМЫ / PLASMA PHYSICS

DOI: <https://doi.org/10.60797/IRJ.2024.145.28>

2D SIMULATION OF THE AC ARGON PLASMA JET AT LOW TEMPERATURE USING COMSOL MULTIPHYSICS SOFTWARE

Research article

Takouche N.K.^{1,*}, Kashapov R.N.²¹ORCID : 0009-0007-0249-2888;^{1,2}Kazan Federal University, Kazan, Russian Federation

* Corresponding author (ntakouchek[at]gmail.com)

Abstract

In this study, we simulated a two-dimensional physical model of the low temperature plasma jet based on a dielectric barrier discharge, so the mathematical model is solved by the finite element method (FEM) using the commercial FEM solver COMSOL Multiphysics, for a unique geometry in which argon gas is used with an AC power supply, for a voltage of 5 KV amplitude, a pressure of 1 Torr and a frequency of 17 KHz. This made it possible to study the different parameters of the plasma jet, such as electron density, electron temperature distribution, electric field distribution and other characteristics in the reaction chamber. The results show that the maximum electron density is generated at the orifice of the plasma jet at low temperature. The maximum electric field of 1.28×10^7 V/m and the maximum electron density of 3.5×10^{17} (1/m³) are observed. The maximum electric field of 1.28×10^7 V/m near the tube surface causes ionization in the plasma channel to propagate the plasma plume. The simulation made it possible to follow the development of the discharge, the formation of the ionization wave and the surface discharges towards the exit of the tube over time.

Keywords: plasma jet based on a dielectric barrier discharge, electron density, electron temperature.

2D-МОДЕЛИРОВАНИЕ СТРУИ АРГОНОВОЙ ПЛАЗМЫ ПЕРЕМЕННОГО ТОКА ПРИ НИЗКОЙ ТЕМПЕРАТУРЕ С ИСПОЛЬЗОВАНИЕМ ПРОГРАММНОГО ОБЕСПЕЧЕНИЯ COMSOL MULTIPHYSICALS

Научная статья

Такуш Н.К.^{1,*}, Кашапов Р.Н.²¹ORCID : 0009-0007-0249-2888;^{1,2}Казанский Федеральный Университет, Казань, Российская Федерация

* Корреспондирующий автор (ntakouchek[at]gmail.com)

Аннотация

В данном исследовании мы смоделировали двумерную физическую модель низкотемпературной плазменной струи на основе диэлектрического барьерного разряда, так что математическая модель решена методом конечных элементов (МКЭ) с помощью коммерческого алгоритма решения МКЭ COMSOL Multiphysics, для уникальной геометрии, в которой используется газ аргон с источником питания переменного тока, для напряжения амплитудой 5 КВ, давления 1 Торр и частоты 17 КГц. Это позволило исследовать различные параметры плазменной струи, такие как плотность электронов, распределение температуры электронов, распределение электрического поля и другие характеристики в реакционной камере. Результаты показывают, что максимальная электронная плотность генерируется в отверстии плазменной струи при низкой температуре. Наблюдается максимальное электрическое поле $1,28 \times 10^7$ В/м и максимальная плотность электронов $3,5 \times 10^{17}$ (1/м³). Максимальное электрическое поле $1,28 \times 10^7$ В/м вблизи поверхности трубки вызывает ионизацию в плазменном канале для распространения плазменного сгустка. Моделирование позволило проследить развитие разряда, формирование волны ионизации и поверхностных разрядов к выходу из трубки с течением времени.

Ключевые слова: плазменная струя на основе диэлектрического барьерного разряда, плотность электронов, температура электронов.

Introduction

The physics of non-equilibrium plasmas at room temperature is currently the subject of numerous research projects; it's a booming field. Different types of plasma, presenting very different characteristics, can be generated at atmospheric pressure by simply changing the shape of the electrical excitation, the geometry of the reactor or that of the electrodes. At present, cold plasma jets (CPJ) are widely studied, and many applications for these devices have been developed due to their versatility, ease of use and low consumption [21], [24], [28], [29]. Jets have strong application potential in the following fields: industrial, biological, medical and agricultural. Thanks to their low temperature, generally below 40°C, these plasmas can be applied directly to thermosensitive surfaces (such as living cells) without damaging them [1], [3], [11], [15], [23]. There are various types of CPJ based on a dielectric barrier discharge (DBD) with various configurations [4], [12], [14]. These plasma jets are powered by various sources, including microwaves, RF (radio frequency), AC (alternating current), or pulsed power; which operate in the presence of various gases, such as noble gases like helium (He) and argon (Ar), or a mixture of noble gases with a small amount of N₂/O₂ [10], [13], [30]. Among the different Dielectric Barrier Discharge (DBD) configurations, the cylindrical geometry stands out as the most commonly used, as It takes advantage of the gas flow to naturally produce a plasma jet [28]. Numerous studies have been conducted on cold plasma jets using different arrangements. However, there is no

specific configuration considered ideal, even for specific applications [21], [29]. This suggests the need for continued research and innovation in this field.

Indeed, these jets have the capability to generate packets of energetic electrons, which, through the space charge effect, create significant electric fields. These electric fields, lead to the generation of chemically active species through electronic impact with the neutral, molecular and atomic species of the gas. The characteristics of CPJ can be controlled by various operating parameters, including applied voltage, frequency, gas flow, pulse width, and working gas [6], [8], [19], [20]. The described parameters have a significant impact on the discharge behavior and propagation dynamics of CPJs under room temperature conditions. The resulting plasma plume moves at high speed through the air, leaves behind short- and long-lived reactive species. Therefore, a plasma plume is generated by a controlled discharge with varying operational and geometric parameters. Deepak et al. conducted a study on the effect of applied voltage and frequency on the length of the plasma plume generated from DBD-based CPJs [5], [16]. Additionally, Kang et al. [9], demonstrated the effect of tube shape on plasma plume characteristics. These findings highlight the intricate dynamics and controllability of cold plasma jets, and the significant impact of operational parameters on their characteristics and behavior. A key challenge resides in managing and comprehending the interplay among various plasma parameters. With this in mind, the work delves into the electrical traits of the Dielectric Barrier Discharge (DBD) Argon-plasma jet and the plasma species. Utilizing the COMSOL Multiphysics 6.1 package, a 2D simulation was conducted to scrutinize the time-evolving properties of plasma plume formation during the discharge phase. The simulation incorporates reaction rates, including key processes like electron attachment and detachment, and surface charge accumulation to comprehensively analyze plasma plume formation and propagation.

By employing advanced simulation techniques and studying these intricate plasma dynamics, the research aims to enhance understanding and control of plasma parameters for optimized outcomes.

Simulation model and theoretical analysis

2.1. Geometric model

The actuator configuration utilized in the study is illustrated in Figure 1. It comprises a dielectric tube with relative permittivity $\epsilon_r = 2.3$, inner/outer radius 0.2/0.3 cm.

The tube features copper electrodes are wrapped around it : one connected to high voltage (the near end) and the other connected to ground. Electrodes are 0.3 wide and 0.1 cm thick, placed very close to each other and separated by a 0.2 cm wide/thick dielectric. Anode is placed 0.4 cm away from the tube outlet.

The model's transport (mobility and diffusion) and reaction coefficients (in appendices) are dependent on the local reduced electric field E/N ; determined using the Boltzmann equation solver BOLSIG+ [7] (developed by LAPLACE institute). Argon is considered a pure gas at a temperature of 400 K and a pressure 1 Torr. The secondary emission coefficient is set at 0.1 with a continuous electronic background of 10^9 cm^{-3} . The ascending edge of the voltage pulse is approximated by a sinusoidal function $U_{app}(t) = U_{app,max} \sin(2\pi f_0 t)$, where maximum amplitude $U_{app,max}$ is equal to 5kV and frequency $f_0 = 17\text{KHz}$.

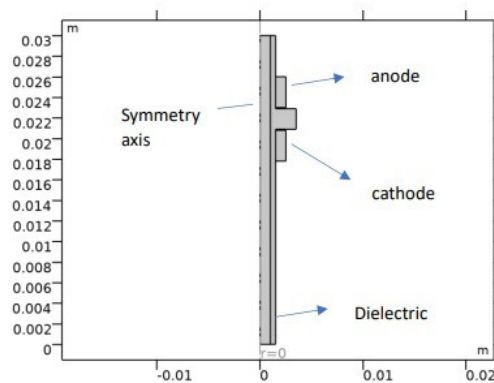


Figure 1 - Simulation geometry

DOI: <https://doi.org/10.60797/IRJ.2024.145.28.1>

Theoretical basis

The foundational plasma module, established on the classical fluid model, intricately encompasses equations comprising: the continuity equation, monitoring the progression of electron density alongside the average electron energy, as well as the multivariate diffusion equation components that drive the evolution of heavy species such as neutral, excited and ionic components. These equations are notably interconnected with the Poisson equation. Equations (1) and (2) represent the continuity and the electron flow equation, respectively:

$$\frac{\partial n_e}{\partial t} + \nabla \cdot \vec{\Gamma}_e = Re - (\vec{u} \cdot \nabla) n_e \quad (1)$$

$$\vec{\Gamma}_e = 1 \cdot (\vec{\mu}_e \cdot \vec{E}) \eta_e - \vec{D}_e \cdot \nabla n_e \quad (2)$$

where n_e characterizes the density of electrons present within the plasma environment, D_e electron diffusion coefficient, and $\vec{\Gamma}_e$ represents the electron flux, \vec{u} average velocity of the species, Re – production rate of electrons.

Electronic flow is made up of two terms; one caused by electric field and others caused by density gradient. Electron energy density equation:

$$\frac{\partial n_e}{\partial t} + \nabla \cdot \vec{\Gamma}_e + \vec{E} \cdot \vec{\Gamma}_e = S_{en} - (\vec{u} \cdot \nabla) n_e + (Q + Q_{gen}) / q \quad (3)$$

$$\vec{\Gamma}_e = - \left(\vec{\mu}_e \cdot \vec{E} \right) \cdot n_e - \vec{D}_e \cdot \nabla n_e \quad (4)$$

This expression $\vec{E} \cdot \vec{\Gamma}_e$ represents the energy received by the electron in each electric field. The energy R_e produced by an inelastic collision is calculated according to the next equation:

$$R_e = S_{en} + \frac{Q - Q_{gen}}{q} \quad (5)$$

By replacing this expression in equation (3) we obtain:

$$\frac{\partial n_e}{\partial t} + \nabla \cdot \vec{\Gamma}_e + \vec{E} \cdot \vec{\Gamma}_e = R_e - (\vec{u} \cdot \nabla) n_e \quad (6)$$

S_{en} is the gain rate or power dissipation when an electron collides inelastically with heavy species, Q_{gen} is the thermal source and q is the electronic charge, μ_e represents the energy mobility and D_e the energy distribution coefficient. The interconnection among these parameters is depicted in Eq:

$$D_e = \mu_e T ; \quad D_e = \mu_e T e ; \quad \mu_e = \frac{5}{3} \mu_e \quad (7)$$

We employed Townsend coefficients, assuming that the electron source is calculated by :

$$R_e = \sum_{j=1}^M x_j a_j N_n |\Gamma_e| \quad (8)$$

Where M representing the number of reactions, x_j denoting the mole fraction of the target species for reaction j, a_j defines the Townsend coefficient for reaction j, and N_n signifying the total number of neutral particles. Considering p , the number of inelastic electron collisions, we will have:

$$R_e = \sum_{j=1}^P x_j a_j N_n |\Gamma_e| \Delta \varepsilon_j \quad (9)$$

with $\Delta \varepsilon_j$ is the energy dissipation of the jth reaction. For non-electronic species, the next equations are solved for each mass fraction:

$$\rho \frac{\partial w_k}{\partial t} + \rho (\vec{u} \cdot \nabla) w_k = \nabla \cdot \vec{j}_k + R_k \quad (10)$$

in which w_k is the ion density, j_k – energy flux of the ions. The electrostatic field is obtained by the following equation:

$$\nabla \cdot (\varepsilon_0 \varepsilon_r E) = \rho \quad (11)$$

where ε_0 is the vacuum permittivity and ε_r is a relative dielectric constant.

The Maxwellian electronic energy distribution function (EEDF) has the expression:

$$f(\varepsilon) = \varphi^{-\frac{3}{2}} \beta_1 \exp\left(-\left(\frac{\varepsilon \beta_2}{\varphi}\right)\right) \quad (12)$$

With ε is the energy of the electrons (SI unit: eV)

Where:

$$\beta_1 = \Gamma \left(\frac{5}{2}\right)^{\frac{3}{2}} \Gamma \left(\frac{3}{2}\right)^{-\frac{5}{2}} \quad \beta_2 = \Gamma(5/2) \Gamma(3/2)^{-1} \quad (13)$$

Boundary condition

Regarding the boundary conditions of the electronic flux and the energy flux, the following relationships are obtained:

$$-\hat{n} \cdot \vec{\Gamma}_e = \left(\frac{1}{2} v_{eth} n_e\right) - \sum_P \gamma_P \left(\vec{\Gamma}_P \cdot \hat{n}\right) \quad (14)$$

$$-\hat{n} \cdot \vec{\Gamma}_e = \left(\frac{5}{6} v_{eth} n_e\right) - \sum_P \varepsilon_P \gamma_P \left(\vec{\Gamma}_P \cdot \hat{n}\right) \quad (15)$$

The second term on the right side of the equation (14) illuminates the electron-induced phenomena predicated upon secondary emission and γ is the secondary emission coefficient. On the electrode surface, ions and excited species are neutralized by surface reactions. Surface interactions on the electrodes are simulated using the coefficient β_j , which determines the probability of operating on j species. The general equation for species k is given by:

$$\rho \frac{\partial (w_k)}{\partial t} = \nabla \cdot j_k + R_k$$

$$j_k = \rho w_k V_k \quad (16)$$

the transport equation concerning the neutral, excited species is::

$$V_k = D_{k,m} \nabla \ln(w_k) + D_{k,m} \nabla \ln(M_n) + \frac{D_n^T}{\rho w_k} \nabla \ln(T) - Z_k \mu_{k,m} E \quad (17)$$

With: j_k is the diffusive flux vector, R_k is the expression of the rate for the species k (SI unit: kg/(m³·s)), ρ designates the density of the mixture (SI unit: kg/m³), and w_k is the mass fraction of the kth species;

$D_{k,m}$ is the averaged diffusion coefficient of the mixture (SI unit: m²/s)

D_n^T the thermal diffusion coefficient for the species k (SI unit: kg/(m·s))

$\mu_{k,m}$ is the average mobility of the mixture for species k (SI unit: m²/(V·s))

The reactions due to electronic impact inside the gas space are presented in Tables 1 [31] (see appendices).

In the majority of research conducted within this domain, a reaction has been used to simplify the calculations. However, the inclusion of additional reactions can extend the computational time required. Apart from the seven previously mentioned reactions, the incorporation of two surface reactions is also taken into consideration, as delineated in Table 2 [31] (Appendices).

Simulation results

Based on the work of Pawalt et al. [17]; we used the parameters of close simulations and those experimental ones that they describe. As discharge gas, we used pure argon. The numerical computations were conducted through the finite element method (FEM) using the COMSOL Multiphysics 6.1 commercial solver. The generation of cold, stable plasmas at room temperature can be achieved by transferring electrical energy to the discharge via the acceleration of charged species through the applied electric field [25], [26], [27]. The outcomes pertain to the initiation of the discharge at the electrodes and its propagation inside to the end of the tube.

The observations presented in Figure 2 reveal an electron density distribution between the anode and cathode, attaining a peak value of $3.5 \times 10^{17} \text{ m}^{-3}$. Notably, a localized region of elevated electron density emerges in close proximity to the cathode. This augmentation in electron density is attributed to electronic avalanches occurring in the vicinity of the high voltage-connected electrode (between $1\text{E-}5 \text{ s}$ and $1\text{E-}3 \text{ s}$). The electrons migrate towards the high voltage-connected electrode, leaving behind a positive space charge which distorts the geometric field. An ionization wave emerges around the symmetry axis and moves towards the tube exit, leading to a continuous rise in electron density. However, this avalanche discharge is not perpetual, as the electric field essentially approaches zero, causing a decrease in electron density, as depicted in the graph in Figure 3.

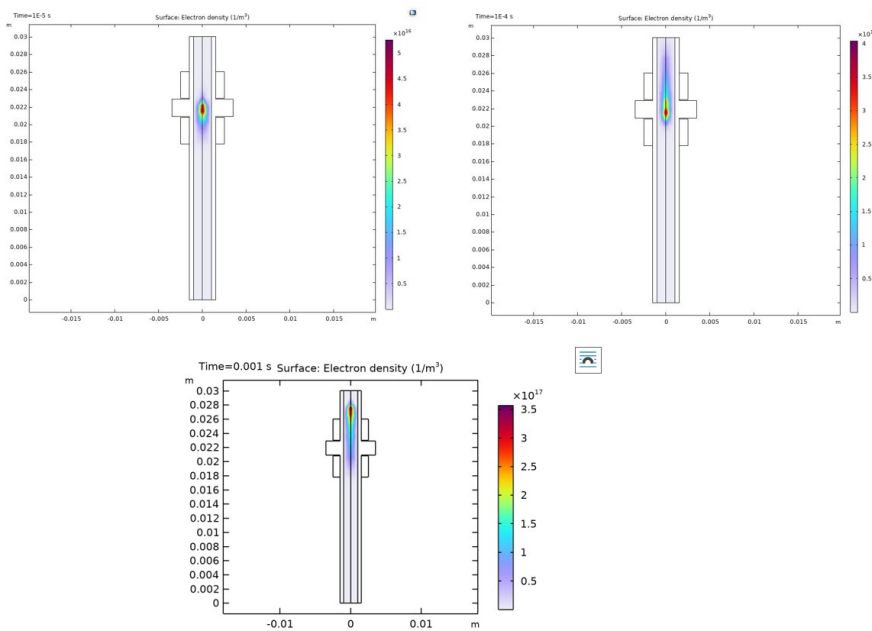


Figure 2 - The evolution of the electron density (m^{-3}) between the electrodes. The high voltage electrode is on top and the ground electrode is on the bottom

DOI: <https://doi.org/10.60797/IRJ.2024.145.28.2>

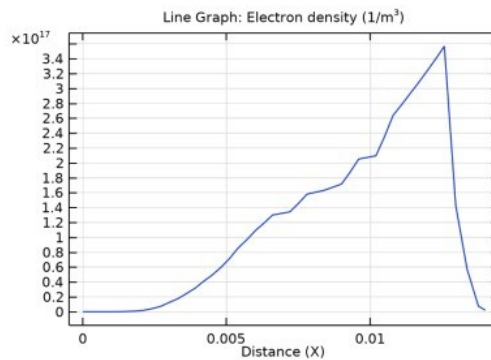


Figure 3 - Curve of the evolution of the electron density (m^{-3})

DOI: <https://doi.org/10.60797/IRJ.2024.145.28.3>

The electric field under the electrodes is equal to zero because of the annular shape of the electrodes (which form Faraday cages) but it is maximum on the edges of the high voltage-connected electrode with a value of the order of 10^7 (V/m) figure 4. This electric field amplitude is sufficient to generate high ionization processes.

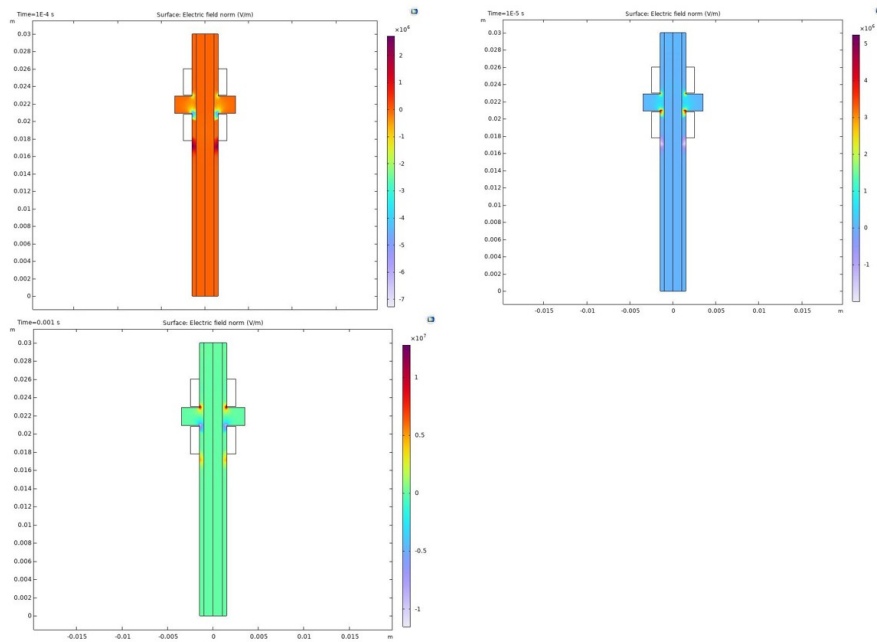


Figure 4 - Electric field in the tube
 DOI: <https://doi.org/10.60797/IRJ.2024.145.28.4>

Due to secondary emission electronic processes, a ring-shaped surface discharge forms and propagates beneath the mass between 10^{-5} s and 10^{-4} s (see Figure 2 and 4). The electron density and the reduced electric field remain high enough to bring this wave to the exit of the electrode, then to the edge of the dielectric tube at 10^{-3} s.

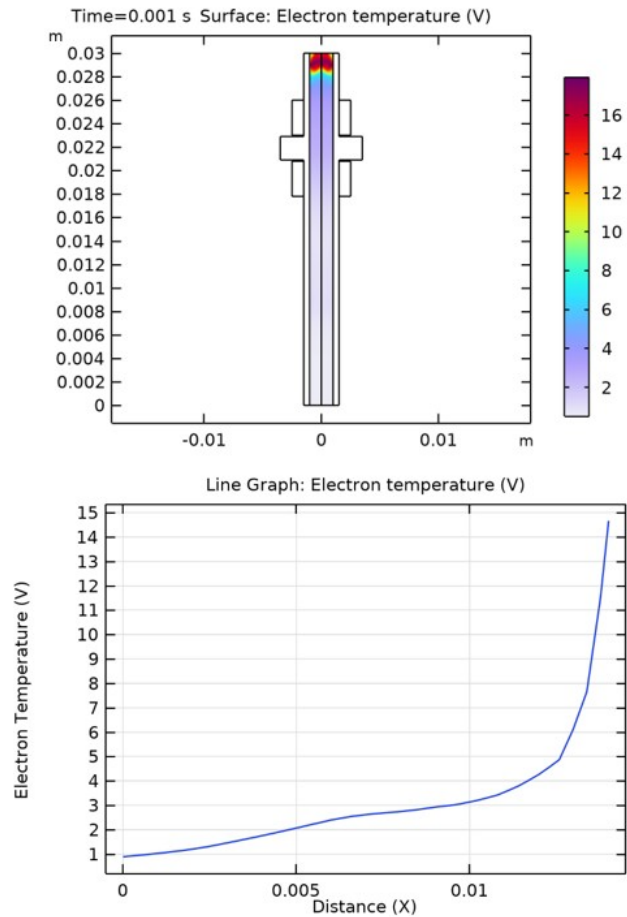


Figure 5 - Simulation of the electronic temperature distribution of Ar and the curve
 DOI: <https://doi.org/10.60797/IRJ.2024.145.28.5>

We note that the maximum electronic temperature is 17.9eV for a duration of 10^{-3} s and progresses until the exit of the tube as illustrated in the graph. Under the influence of an electric field, electrons and ions migrate toward the anode and cathode, respectively, resulting in the formation of space charge regions near the electrodes. Owing to their significantly lower drift velocities, ions exhibit markedly higher charge densities than electrons within the space charge region. This leads to a concentration of the voltage drop between the anode and cathode, as depicted in Figure 5.

The mass fraction of excited Ar atoms is more concentrated in the region near the symmetry axis than at the accumulation surface, specifically at the level of the dielectric walls. Excited species exhibit a longer lifetime in this interval compared to ions and electrons

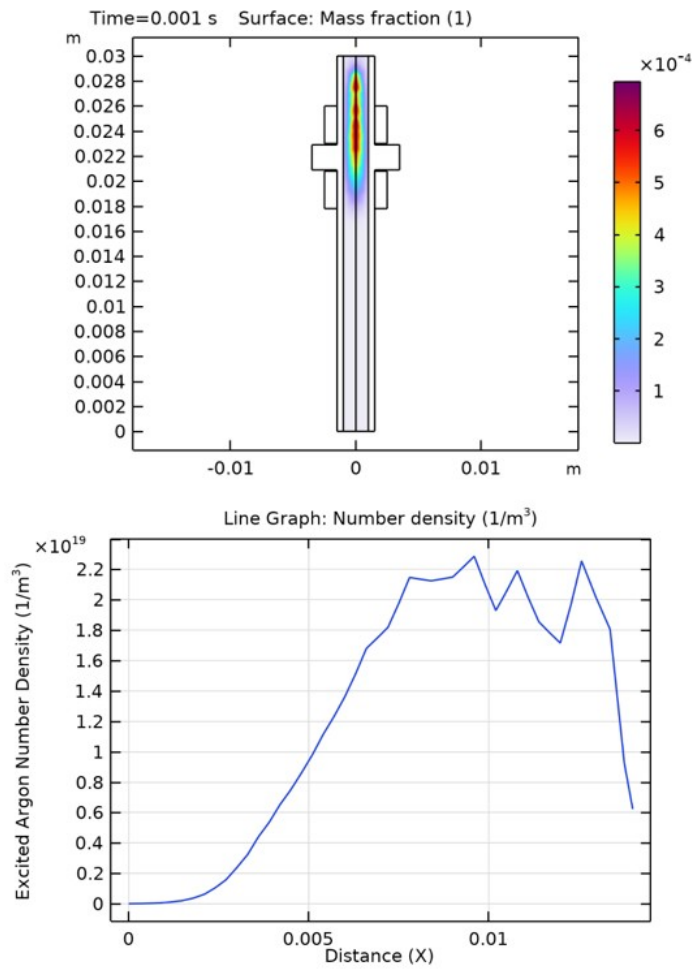


Figure 6 - Mass fraction and density number of argon excites
 DOI: <https://doi.org/10.60797/IRJ.2024.145.28.6>

The variation in number of Argon ion density and concentration in the medium is shown in Figure 7.

Figure 8 shows distribution of total conduction current density excluding the first cycle, conservation of charge across space.

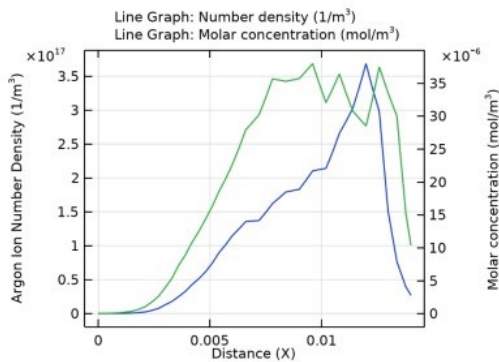


Figure 7 - Number density (1/m³) AND: Molar concentration (mol/m³)
 DOI: <https://doi.org/10.60797/IRJ.2024.145.28.7>

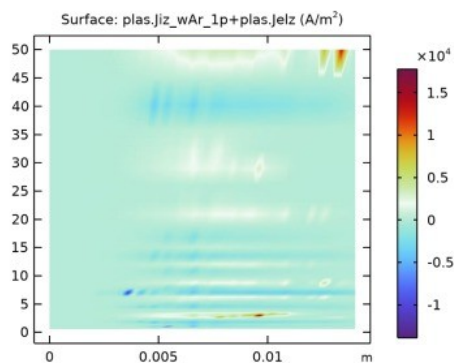


Figure 8 - Total Conduction Current Density
DOI: <https://doi.org/10.60797/IRJ.2024.145.28.8>

Conclusion

Simulation analysis has been conducted to evaluate the characteristics of an Argon plasma jet at room temperature, utilizing a ring electrode configuration via the dielectric barrier discharge (DBD) method, and employing the finite element method for precise calculations. The underlying mathematical model relies on the Boltzmann transport equation to accurately depict the transient physical properties of plasma produced by an Argon discharge. The plasma simulation study focused on examining the propagation characteristics of the plasma plume within the low-temperature plasma jet. This approach facilitated a detailed examination of various PJ parameters, encompassing electron density, electron temperature distribution, and electric field distribution within the reaction chamber. Notably, the highest electron density was observed at the orifice of the plasma jet at room temperature. Key findings include a maximum electric field intensity of 1.28×10^7 V/m and a peak electron density of 3.5×10^{17} m⁻³. The substantial electric field near the tube surface, measuring 1.28×10^7 V/m, contributes significantly to ionization within the plasma channel, thereby advancing the propagation of the plasma plume. The results from the simulation indicate that the mathematical model effectively captures the variations in electron density within the chamber, demonstrating a continuous increase and migration of electron density from the cathode to the anode, proceeding towards the exit over time.

In conclusion, the two-dimensional mathematical fluid model, based on the finite element method, proves to be an effective tool for simulating plasma in an AC discharge plasma jet device across a broad range of parameters. This methodology holds great promise for reactor development pertinent such as our, to diverse applications in sectors such as agriculture, medicine, and biomedical fields, offering significant potential benefits.

Конфликт интересов

Не указан.

Рецензия

Канарейкин А.И., Российский государственный геологоразведочный университет имени Серго Орджоникидзе, Москва, Российская Федерация
DOI: <https://doi.org/10.60797/IRJ.2024.145.28.9>

Conflict of Interest

None declared.

Review

Kanareikin A.I., Russian State Geological Prospecting University named after Sergo Ordzhonikidze, Moscow, Russian Federation
DOI: <https://doi.org/10.60797/IRJ.2024.145.28.9>

Список литературы на английском языке / References in English

1. Khlyustova A. Important parameters in plasma jets for the production of RONS in liquids for plasma medicine: A brief review / A. Khlyustova, C. Labay, Z. Machala et al. // *Front. Chem. Sci. Eng.* — 2019. — 13(2):238–252
2. Lay B. Breakdown processes in metal halide lamps / B. Lay, R.S. Moss, S. Rauf et al. // *Plasma Sources Sci. Technol.* — 2003. — 12, 8.
3. Duřsan Bran'ý. Cold Atmospheric ~ Plasma: A Powerful Tool for Modern Medicine / Duřsan Bran'ý, Dana Dvorská, Erika Halařsov'á [et al.] // *International Journal of Molecular Sciences*, 21(8):2932, January 2020. Number: 8 Publisher: Multidisciplinary Digital Publishing Institute.
4. Xu G. M. DBD plasma jet in atmospheric pressure argon / G. M. Xu, Y. Ma, G. J. Zhang // *IEEE Trans. Plasma. Sci.* — 2008. — 36, 1352. DOI: 10.1109/TPS.2008.917772.
5. Deepak G.D. The effect of mixed electric field on characteristic of Ar–N₂ plasma jets for TiN surface treatment / G.D. Deepak, N.K. Joshi, R. Prakash [et al.] // *Phys. J. Appl. Phys.* 83, 20801 (2018) DOI 10.1088/1361-6463/ab5ee1
6. Deepak G.D. A low power miniaturized dielectric barrier discharge based atmospheric pressure plasma jet Laser Part / G. D. Deepak, N. K. Joshi, U. N. Pal [et al.] // *Beams* 34, 615 (2016).
7. Hagelaar G.J.M. Solving the Boltzmann equation to obtain electron transport coefficients and rate coefficients for fluid models / G.J.M. Hagelaar, L. C. Pitchford // *Plasma Sources Sci. Technol.* — 2005. — Vol. 14. — p. 722-733.
8. Joh H.M. Electrical and Optical Characterization of Atmospheric-Pressure Helium Plasma Jets Generated With a Pin Electrode: Effects of the Electrode Material, Ground Ring Electrode, and Nozzle Shape / H.M. Joh, H.R. Kang, T.H. Chung et al. // *IEEE Trans. Plasma Sci.* — 2014. — 42, 3656. DOI: 10.1109/TPS.2014.2332171.

9. Kang H.R. Effects of dielectric tube shape and pin-electrode diameter on the plasma plume in atmospheric pressure helium plasma jets / H.R. Kang, T.H. Chung, H.M. Joh et al. // *IEEE Trans. Plasma Sci.* — 2017. — 45, 691 .
10. Lee H.W. Distinctive plume formation in atmospheric Ar and He plasmas in microwave frequency band and suitability for biomedical applications *Phys* / H. W. Lee, S. K. Kang, I. H. Won [et al.] // *Plasmas* 20, 123506 (2013).
11. Adamovich I. The 2017 Plasma Roadmap: Low temperature plasma science and technology. / I. Adamovich, S. D. Baalrud, A. Bogaerts et al. // *J. Phys. D: Appl. Phys.* — 2017. — 50(32):323001.
12. Kolb J. Cold atmospheric pressure air plasma jet for medical applications / J. Kolb, A. Mohamed, R. Price et al. // *Appl. Phys Lett.* — 2008. — 92, 241501.
13. Lim J.P. Influence of oxygen in atmospheric-pressure argon plasma jet on sterilization of *Bacillus atropheus* spores / J. P. Lim, H. S. Uhma, S. Z. Li. // *Phys. Plasmas* 14, 093504 (2007).
14. Walsh J. Room-temperature atmospheric argon plasma jet sustained with submicrosecond high-voltage pulses. / J. Walsh, M. Kong // *Appl. Phys. Lett.* — 2007. — 91, 221502. DOI: 10.1063/1.2817965..
15. Laroussi Mounir. Cold Plasma in Medicine and Healthcare: The New Frontier in Low Temperature Plasma Applications / Mounir Laroussi // *Front. Phys.*, 8, 2020. Publisher: Frontiers.
16. Seddaoui N. Atmospheric pressure plasma jet based on the dielectric barrier discharge / N. Seddaoui, M. Ouali, Y.Lagmich // *ITM Web of Conferences* 48, 02008 (2022). — DOI: 10.1051/itmconf/2 224802008 ICCWCS 202
17. Pawłat J. Effects of atmospheric pressure plasma jet operating with DBD on *Lavatera thuringiaca* L. seeds' germination / J. Pawłat, A. Starek, A. Sujak et al. // *PLoS ONE* . — 2018. — 13(4): e0194349. DOI: 10.1371/journal.pone.0194349.
18. Gulati P. Ultraviolet-B radiation enhancement in dielectric barrier discharge based xenon chloride exciplex source by air / P. Gulati, R. Prakash, U.N. Pal et al. // *Appl. Phys. Lett.* — 2014. — 105, 013505.
19. Zhang P. Two-dimensional numerical study of atmospheric pressure glows in helium with impurities / P. Zhang, U. Kortshagen // *J. Phys.* — 2006. — D 39, 153. DOI: 10.1088/0022-3727/39/1/023.
20. Mehrabifard R. Two-dimensional simulation of argon dielectric barrier discharge (DBD) plasma actuator with COMSOL Multiphysics / R. Mehrabifard // *s. Radiation Physics and Engineering.* — 2023. — 4(4):. — p. :43–50.
21. Brandenburg R. Dielectric barrier discharges: progress on plasma sources and on the understanding of regimes and single filaments / R. Brandenburg // *Plasma Sources Sci. Technol.* — 2017. — 26(5):053001.
22. Rai S.K. , A compact nanosecond pulse generator for DBD tube characterization / S.K. Rai, A.K. Dhakar, U.N. Pal // *Rev. Sci. Instrum.* — 2018. — 89, 033505.
23. Reuter Stephan The kINPen—a review on physics and chemistry of the atmospheric pressure plasma jet and its applications / Stephan Reuter, Thomas von Woedtke, Klaus-Dieter Weltmann // *J. Phys. D: Appl. Phys.* — 2018. — 51(23):233001,.
24. Ulrich Kogelschatz. Dielectric-Barrier Discharges: Their History, Discharge Physics, and Industrial Applications. *Plasma Chemistry and Plasma Processing*, 23(1):1–46, March 2003.
25. Pal U.N. Analysis of Power in an Argon Filled Pulsed Dielectric Barrier Discharge / U.N. Pal, P. Gulati, R. Prakash et al. // *Plasma Sci. Technol.* — 2003. — 15, 635. DOI: 10.1088/1009-0630/15/7/06.
26. Pal U.N. Analysis of discharge parameters and optimization study of coaxial DBDs for efficient excimer light sources / U.N. Pal, P. Gulati, M. Kumar et al. // *Theor. Appl. Phys.* — 2012. — 6, 41.
27. Pal U.N. Multiswitch equivalent electrical model to characterize coaxial DBD tube / U N. Pal, P. Gulati, N. Kumar et al. // *IEEE Trans. Plasma Sci.* — 2012. — 40, 1356.
28. X. Lu. Guided ionization waves: Theory and experiments / X. Lu, G. V. Naidis, M. Laroussi [et al.] // *Physics Reports*, 540(3):123–166, July 2014
29. Lu XinPei L. Guided ionization waves: The physics of repeatability / XinPei L. Lu, Kostya Ostrikov // *Applied Physics Reviews*, Publisher: American Institute of Physics. — 2018. — 5(3):031102,.
30. Fua W. A high efficiency low-temperature microwave-driven atmospheric pressure plasma jet / W. Fua, C. Zhanga, C. Nie et al. // *Appl. Phys. Lett.* — 2019. — 114, 254106. DOI: 10.1063/1.5108538.
31. COMSOL Multiphysics 5.4-Plasma Module Library Models. — 2020. — URL: <https://cn.comsol.com/model/dc-glow-discharge-8640> (accessed: 01.04.2024).